and elemental analysis[11] were obtained by this method. For spectral studies described below, Mn(salen)(OC_6H_5) and Mn(salen)(O-*p*-$C_6H_4NO_2$) were prepared by addition of the appropriate phenolate anion to Mn(salen)Cl in MeOH.

The structure of **1**, shown in Figure 1, consists of a five-coordinate Mn(III) atom lying 0.305 Å out of the salen N_2O_2 plane and axially ligated by a thiolate sulfur atom from $^-$S-*p*-$C_6H_4NO_2$. The corresponding out-of-plane displacement in the structure of Mn(salen)Cl is 0.19 Å.[12] Mn-O and Mn-N distances in **1** (see Figure 1 caption) are comparable to those in other Mn(salen)X structures (X = Cl,[12] OAc[13]). The Mn-S bond in **1** is substantially longer than those found in several other manganese(III) thiolate complexes[7] due to its axial postion in this Jahn-Teller-distorted d^4 system. In the structures of $(Et_4N)_2[Mn_2(edt)_4]$,[7a,b] however, one of the unique Mn-(μ-S) bond distances was determined to be 2.606 (2) Å[7a] in one case and 2.632 (2) Å[7b] in the other. Long M-S distances have also been observed in five-coordinate d^9 thiolate complexes.[14] The Mn-Cl distance in Mn(salen)Cl (2.461 Å)[12] is quite close to the Mn-S separation in **1**. The Mn-S-C angle is in between the values for two other transition-metal complexes of $^-$S-*p*-$C_6H_4NO_2$.[15] In contrast to other transition-metal salen species,[16] **1** is mononuclear in the solid state with the closest Mn···Mn separation being 4.14 Å.

Solution stability of **1** is rather limited under normal synthetic conditions, as **1** decomposes with a half-life of 9 min in DMF solution in the presence of room light. In the dark this decomposition is substantially slower; thus, millimolar solutions have a half-life of several hours. Because of this instability, initial characterization of the complex was carried out by using solid samples. Preliminary susceptibility measurements on polycrystalline **1** yielded a magnetic moment of 4.71 μ_B at 281 K, slightly lower than the spin-only value for the high-spin d^4 configuration normally observed for mononuclear Mn(III) complexes.[17] Solid-state reflectance spectra were measured for **1** as well as for a number of other Mn(salen)X complexes including those with X = Cl, OPh, and O-*p*-$C_6H_4NO_2$. All four of these complexes display low-energy absorption bands in the range 620-880 nm.[18] Maxima in this region of the electronic spectrum, as well as at somewhat lower energies, have been assigned to the $^5B_{1g} \rightarrow {}^5A_{1g}$ transition in D_{4h} symmetry for a number of six-coordinate Mn(III) complexes.[19] Several five-coordinate species also displays absorption bands in this spectral region.[19] This transition is considered to correspond to the separation between $d_{x^2-y^2}$ and d_{z^2} orbitals in these Jahn-Teller-distorted d^4 systems. A band at 1160 nm has been reported for Mn(PAP),[4a] outside of the range yet observed for five-coordinate complexes, but consistent with six coordination. The four Mn(salen)X compounds also display shoulders in the region 480-550 nm that are obscured by charge transfer transitions. The position of these bands is consistent with higher energy d-d transition observed for Mn(III) species. Further studies will be required to fully assign the electronic spectra.

In conclusion, a Mn(III) complex of limited stability that incorporates the donor ligands proposed for sweet potato PAP, including a monodentate thiolate group, has been prepared and characterized in the solid state by X-ray crystallography and several physical methods. Compound **1** and related complexes display low-energy electronic absorptions that can be assigned to a transition between d_{z^2} and $d_{x^2-y^2}$ orbitals. Further model studies of this type promise to improve our understanding of the coordination environment and electronic structure of Mn(PAP) and other manganese-containing enzymes.

Acknowledgment. This work was supported by the Searle Scholars Program/The Chicago Community Trust. We thank W. C. A. Wilisch for assistance with the crystal structure determination and H.-C. zur Loye for supplying magnetic data.

Registry No. **1**, 114094-57-4; Mn(salen)(OC_6H_5), 114094-58-5; Mn(salen)(O-*p*-$C_6H_4NO_2$), 114094-59-6; Mn(salen)OAc, 51436-86-3; Mn(salen)Cl, 53177-12-1; acid phosphatase, 9001-77-8.

Supplementary Material Available: Tables of atomic positional and thermal parameters for compound **1** (3 pages). Ordering information is given on any current masthead page.

Department of Chemistry
University of California
Berkeley, California 94720

Joel W. Gohdes
William H. Armstrong*

Received September 17, 1987

(11) Anal. Calcd for $C_{23}H_{20}N_3O_4Cl_2SMn$: C, 49.30; H, 3.60; N, 7.50; Cl, 12.65; S, 5.72; Mn, 9.80. Found: C, 49.39; H, 3.66; N, 7.37; Cl, 12.00; S, 5.85; Mn, 9.59.
(12) Pecoraro, V. L.; Butler, W. M. *Acta Crystallogr., Sect. C: Cryst. Struct. Commun.* **1986**, *C42*, 1151-1154.
(13) Davies, J. E.; Gatehouse, B. M.; Murray, K. S. *J. Chem. Soc., Dalton Trans.* **1973**, 2523-2527.
(14) Anderson, O. P.; Perkins, C. M.; Brito, K. K. *Inorg. Chem.* **1983**, *22*, 1267-1273.
(15) (a) Tang, S. C.; Koch, S.; Papaefthymiou, G. C.; Foner, S.; Frankel, R. B.; Ibers, J. A.; Holm, R. H. *J. Am. Chem. Soc.* **1976**, *98*, 2414-2434. (b) Thompson, J. S.; Marks, T. J.; Ibers, J. A. *J. Am. Chem. Soc.* **1979**, *101*, 4180-4192.
(16) (a) Gerloch, M.; Mabbs, F. E. *J. Chem. Soc. A* **1967**, 1900-1908. (b) Hall, D.; Waters, T. N. *J. Chem. Soc.* **1960**, 2644-2648. (c) Calligaris, M.; Minichelli, D.; Nardin, G.; Randaccio, L. *J. Chem. Soc. A* **1971**, 2720-2724. (d) Mn(salen)Br is probably dimeric based on its magnetic properties. See ref 21.
(17) Kennedy, B. J.; Murray, K. S. *Inorg. Chem.* **1985**, *24*, 1557-1560.
(18) Diffuse reflectance data (nm) for Mn(salen)X compounds: X = Cl, 480 sh, 620; X = OC_6H_5, 480 sh, 800; X = O-*p*-$C_6H_4NO_2$, 500 sh, 770; X = S-*p*-$C_6H_4NO_2$, 550 sh, 880.
(19) (a) Davis, T. S.; Fackler, J. P.; Weeks, M. J. *Inorg. Chem.* **1968**, *7*, 1994-2002. (b) Lever, A. B. P. *Inorganic Electronic Spectroscopy*; Elsevier: Amsterdam, 1984; pp 433-436.

Photodynamics of a Nickel Hydrocorphinoid Model of F_{430}

Sir:

A nickel hydrocorphinoid derivative called F_{430} has recently been identified at the active site of methyl coenzyme M methylreductase (from *Methanobacterium thermoautotrophicum*) and its structure (**1**) has been determined.[1-6] This enzyme catalyzes the final step in the complex series of reactions in the production of methane from carbon dioxide and hydrogen. The potential utility of this process for the chemical or photochemical production of fuels and the catalytic activation of C-H bonds makes the understanding of the mechansims of nickel hydrocorphinoid function of great interest.

Although the hydrocorphinoids are tetrapyrroles, the F_{430} centers in the methyl reductase enzymatic cycle exhibit some unusual properties relative to nickel porphyrins. These include the following: (1) F_{430} can be electrochemically reduced to Ni(I) unlike the more highly conjugated nickel porphyrins, which undergo ring reduction;[7] (2) F_{430} has higher affinity for weak-field axial ligands than most nickel porphyrins;[8-10] and (3) F_{430} has a much greater macrocycle flexibility than nickel porphyrins.[10]

Here we report the results of transient Raman studies of the photodynamics of four- and six-coordinate complexes of a nickel hydrocorphinoid related to F_{430} (see Figure 1). While F_{430} has no in vivo photochemical function, the characterization of ex-

(1) Gunsalus, R. P.; Wolfe, R. S. *FEMS Microbiol. Lett* **1978**, *3*, 191.
(2) Diekert, G.; Klee, B.; Thauer, R. K. *Arch. Microbiol.* **1980**, *124*, 103.
(3) Whitman, W. B.; Wolfe, R. S. *Biochem. Biophys. Res. Commun.* **1980**, *92*, 116.
(4) Pfaltz, A.; Juan, B.; Fassler, A.; Eschenmoser, A.; Jaenchen, R.; Gilles, H. H.; Diekert, G.; Thauer, R. K. *Helv. Chim. Acta* **1982**, *65*, 828.
(5) Livingston, D. A.; Pfaltz, A.; Schreiber, J.; Eschenmoser, A.; Ankel-Fuchs, D.; Moll, J.; Jaenchen, R.; Thauer, R. K. *Helv. Chim. Acta* **1984**, *67*, 334.
(6) Hausinger, R. P.; Orne-Johnson, W. H.; Walsh, C. *Biochemistry* **1984**, *23*, 801.
(7) Juan, B.; Pfaltz, A. *J. Chem. Soc., Chem. Commun.* **1986**, 1327.
(8) Johnson, A. P.; Wehrli, P.; Fletcher, R.; Eschenmoser, A. *Angew. Chem., Int. Ed. Engl.* **1986**, *7*, 622.
(9) Shelnutt, J. A.; Shiemke, A. K.; Scott, R. A., unpublished results.
(10) Eschenmoser, A. *Ann. N.Y. Acad. Sci.* **1986**, *471*, 108.

0020-1669/88/1327-1842$01.50/0

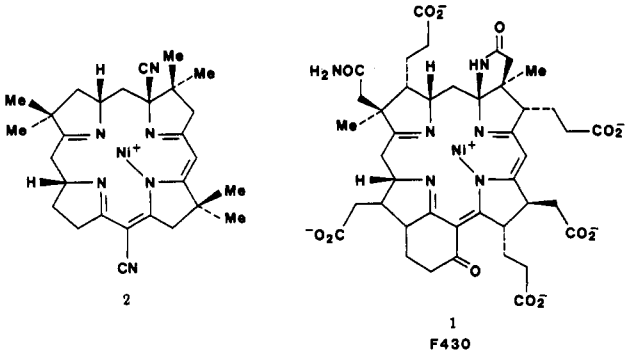

Figure 1. Structures of a nickel hydrocorphinoid model (**2**) and F_{430} (**1**) of methylreductase.

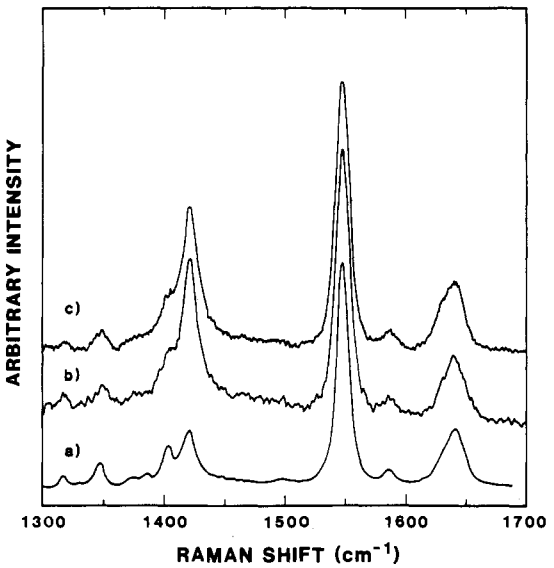

Figure 2. Resonance Raman spectra of **2** in methylene chloride generated within 10 ns of photoexcitation at 410 nm: (a) steady-state spectrum; (b) low-power excitation spectrum (power 0.1 mJ/pulse); (c) high power excitation spectrum (power 1.0 mJ/pulse). For both b and c, the spectral band-pass was 7 cm^{-1} and the laser was operated at a 15 Hz repetition rate.

cited-state structures and dynamics has proven to be a valuable tactic in the study of metalloporphyrins. Recently, the vibrational characteristics of the equilibrium species of the nickel hydrocorphinoid **2** were determined.[11,12] Strong bands in the high-frequency resonance Raman spectra of various ground-state species of **2** were found to respond systematically to nickel ligation state and macrocycle conformation. These data, coupled with recent insights into the transient photoligation behavior of nickel porphyrins obtained in our laboratory and others,[13-20] provide a basis for the interpretation of the transient Raman data gathered from excited-state nickel hydrocorphinoid species. We find the photochemistry of different species of **2** to be quite distinct from that of nickel porphyrin analogues. This suggests that nickel hydrocorphinoids may form a functionally distinct class of prosthetic

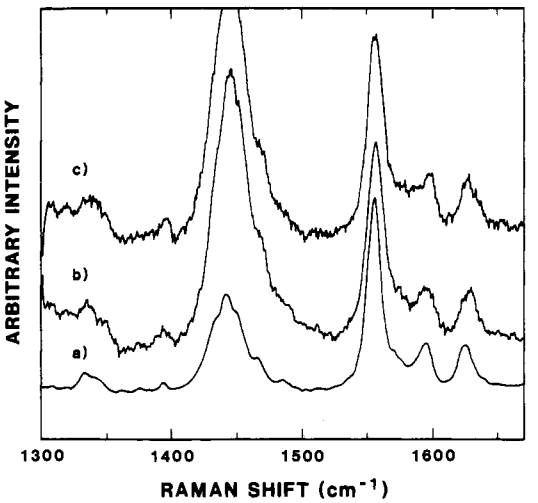

Figure 3. Resonance Raman spectra of **2** in piperidine generated under the same conditions as in Figure 2: (a) steady-state spectrum; (b) low-power excitation spectrum; (c) high-power excitation spectrum.

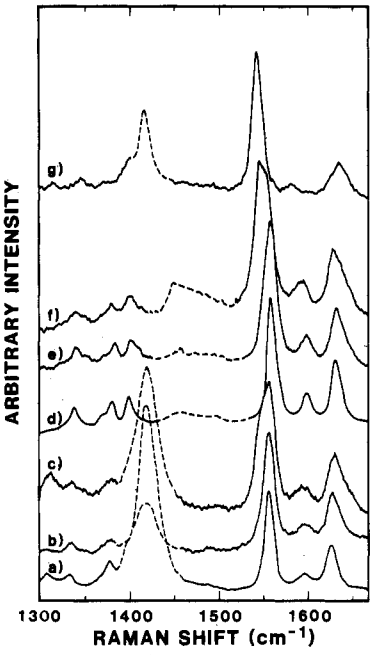

Figure 4. Resonance Raman spectra of photolabile nickel corphinoid species generated under the same conditions as in Figure 1: (a) in DMSO, steady-state conditions; (b) in DMSO, low-power excitation; (c) in DMSO, high-power excitation; (d) in methanol, steady-state conditions; (e) in methanol, low-power excitation; (f) in methanol, high-power excitation; (g) in methylene chloride, low-power excitation. Comparison of spectra c, f, and g shows formation of a four-coordinate excited state in weak ligands DMSO and methanol.

groups with unique dynamic and electronic characteristics.

Materials and Methods. The nickel hydrocorphinoid **2** was prepared as previously described[21] and was graciously provided by Eschenmoser, Pfaltz, and Fässler. Solutions of the hydrocorphinoid were prepared by dissolving it in neat spectral-grade solvents (CH_2Cl_2, pyridine, piperidine, DMSO, or methanol). Ground-state species were characterized by absorption and CW resonance Raman spectroscopies before and after the transient Raman measurements to monitor sample integrity.

The transient Raman spectra were obtained with use of a Molectron UV-24 and a Molectron DL-24 laser system (10-ns nominal pulse width). The output laser beam was imaged on the sample in a backscattering geometry with either a spherical or a cylindrical lens. The scattered radiation was then focused into

(11) Shelnutt, J. A. *J. Am. Chem. Soc.* **1987**, *109*, 4169.
(12) Shelnutt, J. A. submitted for publication in *J. Am. Chem. Soc.*
(13) Findsen, E. W.; Shelnutt, J. A.; Friedman, J. M.; Ondrias, M. R. *Chem. Phys. Lett.* **1986**, *126*, 465.
(14) Findsen, E. W.; Shelnutt, J. A.; Friedman, J. M.; Ondrias, M. R. *ACS Symp. Ser.* **1986**, *No. 321*, 265.
(15) Findsen, E. W.; Shelnutt, J. A.; Alston, K.; Ondrias, M. R. *J. Am. Chem. Soc.* **1986**, *108*, 4009.
(16) Findsen, E. W.; Shelnutt, J. A.; Ondrias, M. R. *J. Phys. Chem.* **1988**, *92*, 307.
(17) Kim, D.-H.; Spiro, T. G. *J. Am. Chem. Soc.* **1986**, *108*, 2099.
(18) Kim, D.-H.; Holten, D. *Chem. Phys.* **1983**, *75*, 305.
(19) Kim, D.-H.; Kirmaier, C.; Holten, D. *Chem. Phys. Lett.* **1983**, *98*, 584.
(20) Kobayashi, T.; Straub, K.; Rentzepis, P. M. *Photochem. Photobiol.* **1979**, *29*, 925.
(21) Fässler, A.; Pfaltz, A.; Krautler, B.; Eschenmoser, A. *J. Chem. Soc., Chem. Commun.* **1984**, 1365.

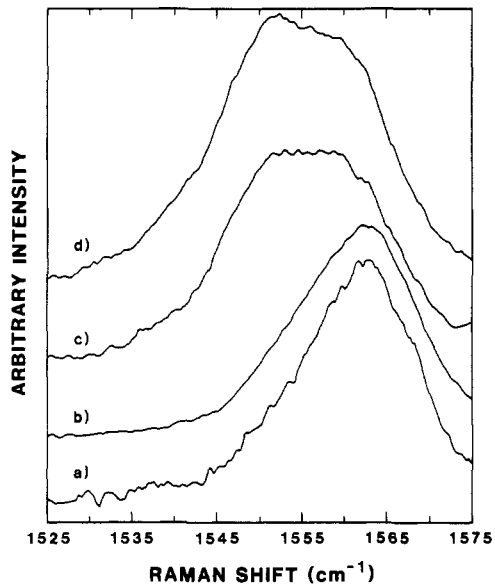

Figure 5. Power dependence profile of photoexcitation of **2** in methanol: (a) low power, power 0.05 mJ/pulse; (b) power 0.1 mJ/pulse; (c) power 0.5 mJ/pulse; (d) power 1.0 mJ/pulse of 410-nm excitation. The power at the sample was modulated by using a combination of spherical and cylindrical optics and neutral density filters. All other conditions were the same as those described in Figure 1.

a SPEX Industries Model 1403 scanning double monochromator and detected with a fast rise time photomultiplier tube (Hamamatsu R928) in a cooled housing. The output of the PMT was directed into an EG&G/PAR Model 162 boxcar with a single plug-in (Model 165). The boxcar signal was then fed into a Datamate Controller (SPEX) for data storage and manipulation.

Laser power densities at the sample were controlled by beam-focusing optics and/or the use of neutral density filters. Low-power spectra were obtained with a cylindrical lens that delivered ~10 mJ/cm^2, high-power spectra with a spherical lens and neutral density filter combination that produced ~100 mJ/cm^2, and very high-power spectra with a tightly focused spherical lens resulting in ~500 mJ/cm^2 at the sample.

Results. Figures 2–5 display resonance Raman spectra of the ground-state four-coordinate and six-coordinate methanol and piperidine complexes of **2** generated within 10 ns of direct photoexcitation of the visible π–π^* transition of the macrocycle (410–440 nm). The dependence of the high-frequency vibrational modes of **2** have recently been characterized and found to be ligation-state dependent. This is particularly true for the prominent modes at 1550–1660 cm^{-1} [11,12] (see Table I).

Spectra identical with those previously obtained for the ground-state species could be produced by using pulsed laser excitation by attenuating the pulse energy (to <0.1 mJ/pulse) with neutral density filters or employing defocused cylindrical optics to direct the beam onto the sample, except for the six-coordinate methanol species, which displayed small shifts in several high-frequency modes even at the lowest excitation energies. All species of **2** examined were found to be nonluminescent. Spectra obtained at higher photon fluxes offer evidence for axial ligand dependent photodynamics of the nickel hydrocorphinoid complexes, which can be contrasted to the photodynamic behavior of the analogous nickel porphyrin complexes.

Strong-field σ-ligands are readily photolyzed from a variety of nickel porphyrins via a metal-centered d–d excited state (see Discussion). Figure 2 demonstrates that such behavior is absent in strong-field six-coordinate complexes of **2**. Neither piperidine nor pyridine (not shown) complexes yield any evidence of phototransient species, even under much higher photon fluxes than those required to completely photolyze analogous porphyrin species.

Four-coordinate **2** also displays no evidence of transient species within the 10-ns laser pulses (see Figure 3). In contrast, nickel porphyrins in noncoordinating solvents or detergent micelles exhibit a solvent-dependent core expansion, resulting from a net $d^2_{z^2} \rightarrow d^1_{x^2-y^2}d^1_{z^2}$ transition.[13–15]

Table I. Nickel(II) Corphinoid Resonance Raman Bands (cm^{-1})[a]

methylene chloride		piperidine	
LP, HP	SS	LP, HP	SS
~1350	1347	~1335	1333
~1380	1384		1375
		1402	~1395
1549	1548	1557	1557
1587	1586	1595	1595
1641	1641	1628	1625

methanol			dimethyl sulfoxide		
SS	LP	HP	SS	LP	HP
1338	1339	1342	1335	~1335	1337
1379	1383	1383	1378	~1379	1381
1398	1402	1404		~1401	
1561	1559	1552, 1558	1557	1559	1557, 1553
1598	1598	1597	1596	1596	1596
1631	1633	1634, 1640[b]	1627	1629[c]	1631

[a] LP = low power (<0.1 mJ/pulse); HP = high power (>1.0 mJ/pulse); SS = steady-state spectra. [b] LP. [c] HP.

In solvents that act as weak field ligands, such as methanol or DMSO, **2** quantitatively forms six-coordinate equilibrium complexes.[10,21,22] Nickel porphyrins, on the other hand, generally exhibit a very low affinity for such ligands. The weak-field hydrocorphinoid complexes display photoinduced transients within 10-ns excitation pulses. For the bis(methanol) and bis(dimethyl sulfoxide) (see Figure 3) complexes, lines at 1552 and ~1640 cm^{-1} appear in the Raman spectra taken at high pulse power along with Raman lines of the ground-state six-coordinate complex at 1559 and 1633 cm^{-1}. The transient species generated in the 10 ns laser pulse is, within experimental error, spectroscopically identical with the four-coordinate equilibrium species (in CH_2Cl_2) and is distinct from the five-coordinate ground-state complexes.[11]

Figure 5 shows that the extent of transient formation is dependent upon laser power and the process is reversible (i.e., low-power spectra obtained subsequent to the high-power spectrum are identical with those of the ground state). Easily detectable quantities of excited-state species could be generated by using either ~410- or ~440-nm excitation. The exact quantification of excited-state yield is, of course, complicated by the uncertainty in the resonance scattering cross sections for the ground- and excited-state species.

Discussion. The data above demonstrates that the photodynamics of nickel hydrocorphinoid species differ from those of analogous nickel porphyrins. However, the existing spectroscopic data indicate that the nickel(II) ion interactions with the macrocycle are qualitatively similar in these systems. Thus, the nickel porphyrins serve as a useful point of comparison for the analysis of nickel hydrocorphinoids.

Ground-State Spectra and Axial Ligation. Nickel(II) porphyrins possess eight metal d electrons, which, in the absence of axial ligands, fill all the nickel d orbitals except the highest lying $d_{x^2-y^2}$ orbital. The presence of strong σ-donating axial ligands raises the energy of the d_{z^2} orbital to the point that $d^1_{z^2}d^1_{x^2-y^2}$ becomes the preferred configuration. This low-spin to high-spin transition upon axial ligation has been verified by NMR spectroscopy.[23] Changes in metal d-orbital occupancy also exert strong influences upon the macrocycle. The dominant porphyrin π–π^* transition (Soret band) shifts from ~400 to ~430 nm upon axial ligand binding.[13–20] Moreover, axial ligation forces an expansion of the porphyrin core (center-to-nitrogen distance).[13–17] This expansion is quite evident in the systematic shift to lower frequency of several high-frequency bands (ν_2, ν_3, ν_{10}, ν_{11}, ν_{19}) of the porphyrin resonance Raman spectrum.

(22) Kratsky, C.; Fässler, A.; Pfeltz, A.; Kräutler, B.; Eschenmoser, A. *J. Chem. Soc., Chem. Commun.* **1984**, 1368.
(23) LaMar, G. N.; Walker, F. A. In *The Porphyrins*; Dolphin, D., Ed; Academic: New York, 1979, Vol. 4.

The nickel(II) ion in **2** is bound in a square-planar fashion similar to the nickel porphyrins and thus exhibits some similarities in its ligation behavior. In the absence of coordinating ligands, **2** is low spin ($S = 0$) while in strong σ-donating solvents, it exhibits $S = 1$ spin[10,21,22] consistent with a $d^1_{z^2}d^1_{x^2-y^2}$ configuration. The addition of strong-field ligands results in shifts in the Soret maximum (from ~410 to ~430 nm) analogous to those observed for nickel porphyrins. Crystallographic studies of complexes related to **2** show that core expansion from ~1.90 to ~2.10 Å also accompanies axial ligation.[22-24]

The differences in macrocycle symmetry and degree of conjugation preclude a direct one-to-one comparison of vibrational modes between hydrocorphinoids and porphyrins. However, studies of the ground-state complexes of **2** by Shelnutt[11,12] have demonstrated that several high-frequency modes of the macrocycle (at 1641, 1548 and 1347 cm^{-1}) respond systematically to axial ligation and conformational changes (see below).

Despite these qualitative similarities, some profound differences between equilibrium species of nickel porphyrins and nickel hydrocorphinoids exist. The most obvious of these is the much greater affinity for weak-field σ-ligands of the nickel hydrocorphinoids. Several recent studies have documented that H_2O, methanol, DMSO, and other weak-field ligands bind readily to **2** and other nickel hydrocorphinoid species,[8,9] producing a red shift (from ~410 to ~430 nm) in the position of the Soret band.[8-12,21,22] Among the porphyrins, only nickel tetrakis(*N*-methylpyridiniumyl)porphyrins display any affinity for these ligands.

Nickel hydrocorphinoids also display a good deal more conformational flexibility than their porphyrin analogues. In particular, the four-coordinate nickel hydrocorphinoids show significant S_4 ruffling in their crystalline forms.[24,26] Recent resonance Raman studies[12] of solution species suggest that multiple conformations of **2** exist at room temperature in noncoordinating solvents.

Photodynamics. The photodynamics of four- and six-coordinate nickel porphyrins have been relatively well characterized by transient absorption[18-20] and resonance Raman[13-17] investigations. Transient absorption data indicate, for both coordination states, that the initial porphyrin $\pi-\pi^*$ excited state decays within a few picoseconds to a metal-centered excited state involving a net d–d transition.[18,19]

For four-coordinate nickel porphyrins, this amounts to a $d^2_{z^2}$ ($^1A_{1g}$) to $d^1_{z^2}d^1_{x^2-y^2}$ ($^3B_{1g}$) transition while a net $^3B_{1g}$ to $^1A_{1g}$ transition occurs in six-coordinate complexes.

Creation of the phototransient $^1A_{1g}$ state leads to dissociation of σ-ligands from the six-coordinate species. The lifetime of the $^1A_{1g}$ excited state in coordinating solvents is ≤2 ns and is probably dictated by either ligand diffusion rates or activation energetics for religation.

Population of the $d_{x^2-y^2}$ orbital in the four-coordinate species results in porphyrin core expansion of ~0.05 Å.[16] The lifetime of this $^*B_{1g}$ excited state is ≤300 ps. The structural effects of the metal-centered d–d transition upon the macrocycle are clearly evident in transient Raman spectra of nickel porphyrins.[13-17]

Our results demonstrate that the photodynamics of nickel hydrocorphinoids are quite distinct from those of nickel porphyrins. Under experimental conditions where nickel protoporphyrin exhibited a significant population of the $^*B_{1g}$ excited state, four-coordinate **2** produced no observable phototransient species. Moreover, piperidine and pyridine could not be photolyzed from six-coordinate complexes of **2** under conditions that produced significant ligand photolysis from porphyrin species. In contrast, the weak-field ligand (methanol, DMSO) complexes of **2** yield phototransients whose spectra were consistent with the photolysis of both axial ligands. The photolysis of weak-field ligands was both reversible and dependent upon laser power (see Figure 5). Thus the photodynamics of weak-field complexes of **2**, mimic, to a large degree, the behavior of six-coordinate complexes of the nickel porphyrins. By analogy with nickel porphyrins, photolysis is most likely initiated via a net $d^1_{x^2-y^2}d^1_{z^2} \rightarrow d^2_{z^2}$ transition at the nickel subsequent to direct photoexcitation of the macrocycle $\pi-\pi^*$ transition.

The absence of observable phototransient species within nanosecond laser pulses for four-coordinate and strong-field ligated species of **2** may result from either a pronounced increase in the rate of radiationless decay from excited states (either the primary $\pi-\pi^*$ state or subsequent d–d excited states) or a reduction in the quantum yield for the creation of the phototransient species relative to nickel porphyrins. Both are viable scenarios for the observed behavior of **2** and could arise from either dynamic or electronic differences between **2** and nickel porphyrins. Qualitative modeling of nickel porphyrin photodynamics[16] indicates that the extent of excited-state formation is an approximately linear function of both quantum yield and excited-state lifetimes.

The molecular dynamics of the hydrocorphinoid macrocycle are undoubtedly different from those of the more rigid porphyrins. Ruffling and other out-of-plane deformations would be expected to be more prominent for the reduced macrocycle of the hydrocorphinoid relative to the porphyrins. The corphin ring is planar in the equilibrium six-coordinate complex,[22] whereas four-coordinate nickel hydrocorphinoids tend to exhibit S_4 ruffling and core contraction.[10,24] These out-of-plane motions might provide relatively efficient pathways for radiationless decay from the metal-centered excited states or lead to direct deactivation of the initial macrocycle $\pi-\pi^*$ state.

Alternatively, the relative energies of the macrocycle π and π^* orbitals and the metal d orbitals might be altered in **2** to the extent that their coupling (either π–d or d–d) is significantly changed, decreasing either the quantum yield for the creation of the metal d–d excited state (if π–d coupling were decreased) or the lifetime of the dissociative excited state (if d–d coupling were increased). Calculations by Chang et al.[27] indicate that the orbital energies of CO complexes of iron chlorins and isobacteriochlorins are qualitatively different from those of iron porphyrins. The macrocycle of **2** is even more reduced than the chlorins, and even larger perturbations of the metal d orbital and macrocycle π orbitals are likely. In view of the dramatically different photodynamics of weak- and strong-field ligand complexes of **2**, it is possible that axial ligand-field strengths could play a pivotal role in the coupling of metal and macrocycle orbitals, thus regulating the photodynamics of the complex.

On the basis of nickel corphin crystal structures, one might expect **2** to convert from a planar structure existing immediately after photoejection of weak-field ligands to a more ruffled, equilibrium structure. Assuming that the Raman spectra of the ruffled and planar four-coordinate species differ (as expected by analogy to nickel porphyrins[28]), the equivalence of the Raman spectra of the transient and four-coordinate equilibrium species requires that the equilibrium structure be attained in less than 10 ns after ligand ejection. On the other hand, four-coordinate nickel hydrocorphinoids might assume a planar conformation under room temperature solution conditions. In that case, no conformational change would occur subsequent to ligand ejection.

In summary, the photodynamic behavior of the nickel hydrocorphinoid **2**, while similar to that for weak-field ligand complexes, differs significantly from that of analogous nickel porphyrins in other respects. Thus, the hydrocorphinoids may form a functionally distinct class of nickel enzyme prosthetic groups in terms of their axial ligation properties. Differences in both the dynamic motion resulting from macrocycle flexibility and electronic structure produced by ring reduction may contribute to their unique photodynamic properties. The protein matrix influences the ground-state structure of F_{430} at the active site of methyl

(24) Kratsky, C.; Waditschatka, R.; August, C.; Johnson, J. E.; Plaquevent, J. C.; Schreiber, J.; Eschenmoser, A. *Helv. Chim. Acta* **1985**, *68*, 1312.
(25) Pasternack, R. F.; Spiro, E. G.; Teach, M. *J. Inorg. Nucl. Chem.* **1974**, *36*, 599.
(26) Waditschatka, R.; Kratsky, C.; Juan, B.; Heinzer, J.; Eschenmoser, A. *J. Chem. Soc., Chem. Commun.* **1985**, 1604.
(27) Chang, C. K.; Hanson, L. K.; Richardson, P. F.; Young, R.; Fajer, J. *Proc. Natl. Acad. Sci. U.S.A.* **1981**, *78*, 2652.
(28) Spaulding, L. D.; Chang, C. C.; Yu, N.-T.; Felton, R. H. *J. Am. Chem. Soc.* **1975**, *97*, 2517.

reductase.[29] It may also affect the photodynamics of its nickel hydrocorphinoid chromophore as it does for nickel porphyrin reconstituted hemoglobins.[15,30,31] This aspect of nickel hydrocorphinoid photodynamics is currently being explored in our laboratories.

Acknowledgment. This work was performed at the University of New Mexico and supported by the National Institutes of Health (Grant GM33330), the donors of the Petroleum Research Fund, administered by the American Chemical Society (to M.R.O), DOE (Contract DE-AC04-76DP00789), the Gas Research Institute (Grant 5082-260-0767) to J.A.S), and the Associated Western Universities.

(29) Shiemke, A. K.; Scott, R. A.; Shelnutt, J. A. *J. Am. Chem. Soc.* **1988**, *110*, 1645.
(30) Shelnutt, J. A.; Alston, K.; Ho, J.-Y.; Yu, N.-T.; Yamamoto, T.; Rifkind, J. M. *Biochemistry* **1986**, *25*, 620.
(31) Shelnutt, J. A.; Alston, K.; Findsen, E. W.; Ondrias, M. R.; Rifkind, J. M. *ACS Symp. Ser.* **1986**, *No. 321*, 232.

Department of Chemistry
University of New Mexico
Albuquerque, New Mexico 87131
B. A. Crawford
E. W. Findsen
M. R. Ondrias*

Fuel Sciences Division 6254
Sandia National Laboratories
Albuquerque, New Mexico 87185
J. A. Shelnutt

Received September 23, 1987

Hydride Binding Energies of Boranes

Sir:

Ion/molecule reactions and gas-phase equilibrium measurements have provided an extensive body of accurate thermochemical information for organic and inorganic ions.[1-6] Gas-phase thermochemical data for borohydride negative ions are conspicuously absent, despite the widespread practical significance of borohydride ion chemistry in solution[7-10] and the relative ease of formation of simple borohydride negative ions in mass spectrometer ion sources.[11,12] The reason for this, in part, is the present lack of suitable ion/molecule reactions involving borohydride ions and well-characterized reference species that are necessary for evaluating their heats of formation.

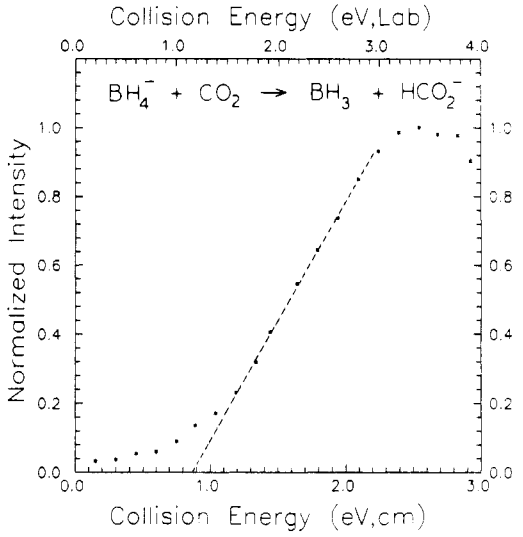

Figure 1. Plot of normalized HCO_2^- ion intensity as a function of BH_4^- ion kinetic energy in the center-of-mass frame (lower scale) and the laboratory frame (upper scale). The dashed line represents a linear fit of the steeply rising portion of the appearance curve.

As part of our ongoing studies of hydride affinities and gas-phase hydride transfer reactions,[13-16] we recently developed a method for estimating hydride binding energies of neutral compounds from endothermic H^- transfer reactions in a flowing-afterglow–triple-quadrupole apparatus. We report here our measurements of the hydride affinity (HA) of BH_3, B_2H_6, and a few of their common derivatives, along with gas-phase heats of formation for the corresponding borohydride negative ions.

All experiments were carried out at 298 ± 2 K in a tandem flowing afterglow–triple-quadrupole instrument recently constructed in our laboratory.[17] Borohydride ions can be synthesized in the helium flow reactor by several different methods. Borane–methyl sulfide ($Me_2S^+-BH_3^-$, BMS) provides a convenient alternative to diborane for the gas-phase synthesis of BH_4^-.[11,12] This volatile Lewis acid–base complex reacts with a variety of pregenerated negative ions (X^-) to yield monosubstituted borohydride ions (XBH_3^-) that undergo further reactions with additional BMS to yield BH_4^- and polyborohydride cluster ions (eq 1). Other substituted borohydride ions can be synthesized from

$$X^- \xrightarrow{BMS} XBH_3^- \xrightarrow{BMS} BH_4^- \xrightarrow{BMS} \rightarrow B_2H_7^-, B_3H_8^- \qquad (1)$$

the corresponding neutral boranes by reactions with hydride donor anions such as $C_5H_{11}SiH_4^-$[16] or c-$C_6H_7^-$[18] (eq 2).

$$n\text{-}C_5H_{11}SiH_4^- + BR_3 \rightarrow HBR_3^- + n\text{-}C_5H_{11}SiH_3 \qquad (2)$$

R = Et, OMe, O-*i*-Pr, F

The BH_4^- and $B_2H_7^-$ ions and most all of the substituted borohydride ions described above are completely unreactive in the

(1) For reviews and data compilations, see: Bartmess, J. E.; McIver, R. T., Jr. In *Gas Phase Ion Chemistry*; Bowers, M. T., Ed.; Academic: New York, 1979; Chapter 11. Lias, S. G.; Liebman, J. F.; Levin, R. D. *J. Phys. Chem. Ref. Data* **1984**, *13*, 695. Kebarle, P. *Annu. Rev. Phys. Chem.* **1977**, *28*, 445. Aue, D. H.; Bowers, M. T. In *Gas Phase Ion Chemistry*; Bowers, M. T., Ed.; Academic: New York, 1979, Chapter 9. Keesee, R. G.; Castleman, A. W., Jr. *J. Phys. Chem. Ref. Data* **1986**, *15*, 1011. Kebarle, P.; Chowdhury, S. *Chem. Rev.* **1987**, *87*, 513.
(2) Larson, J. W.; McMahon, T. B. *J. Am. Chem. Soc.* **1985**, *107*, 766.
(3) Sharma, R. B.; Sen Sharma, D. K.; Hiraoka, K.; Kebarle, P. *J. Am. Chem. Soc.* **1985**, *107*, 3747.
(4) (a) Murphy, M. K.; Beauchamp, J. L. *J. Am. Chem. Soc.* **1976**, *98*, 1433. (b) Murphy, M. K.; Beauchamp, J. L. *J. Am. Chem. Soc.* **1977**, *99*, 4992.
(5) Caldwell, G.; Rozeboom, M. D.; Kiplinger, J. P.; Bartmess, J. E. *J. Am. Chem. Soc.* **1984**, *106*, 4660.
(6) (a) Meot-Ner, M.; Sieck, L. W. *J. Am. Chem. Soc.* **1986**, *108*, 7525. (b) Meot-Ner, M. *J. Am. Chem. Soc.* **1986**, *108*, 6189. (c) Meot-Ner, M. *J. Phys. Chem.* **1987**, *91*, 417.
(7) Brown, H. C. *Boranes in Organic Chemistry*; Cornell University Press: Ithaca, New York, 1972.
(8) Wigfield, D. C. *Tetrahedron* **1979**, *35*, 449.
(9) Wade, R. C.; *J. Mol. Catal.* **1983**, *18*, 273.
(10) Marks, T. J.; Kolb, J. R. *Chem. Rev.* **1977**, *77*, 263.
(11) Dunbar, R. C. *J. Am. Chem. Soc.* **1968**, *90*, 5676.
(12) Enrione, R. E.; Rosen, R. *Inorg. Chim. Acta* **1967**, *1*, 169.
(13) Squires, R. R. In *Structure/Reactivity and Thermochemistry of Ions*; Ausloos, P.; Lias, S. G., Eds.; Reidel: Dordrecht, The Netherlands, 1987; p 373.
(14) Lane, K. R.; Sallans, L.; Squires, R. R. *Organometallics* **1985**, *3*, 408.
(15) Lane, K. R.; Sallans, L.; Squires, R. R. *J. Am. Chem. Soc.* **1985**, *107*, 5369.
(16) Hajdasz, D. J.; Squires, R. R. *J. Am. Chem. Soc.* **1986**, *108*, 3139.
(17) The instrument will be fully described in a subsequent publication. For a preliminary account, see: Squires, R. R.; Lane, K. R.; Lee, R. E.; Wright, L. G.; Wood, K. V.; Cooks, R. G. *Int. J. Mass Spectrom. Ion Processes* **1985**, *64*, 185. Unless otherwise noted the standard experimental conditions are P(He) = 0.40 Torr, F(He) = 190 atm cm^3/s, and v(He) = 9400 cm/s.
(18) DePuy, C. H.; Bierbaum, V. M.; Schmitt, R. J. Shapiro, R. H. *J. Am. Chem. Soc.* **1978**, *100*, 2920.

0020-1669/88/1327-1846$01.50/0